Iron(III) Dopant Counterions Affect the Charge Transport Properties of Poly(thiophene) and Poly(dialkoxythiophene) Derivatives

Khaled Al Kurdi,[†] Shawn A. Gregory,[†] Madeleine P. Gordon, James F. Ponder Jr., Amalie Atassi, Joshua M. Rinehart, Austin L. Jones, Jeffrey J. Urban, John R. Reynolds, Stephen Barlow, Seth R. Marder,[*] Shannon K. Yee[*]

[†] These authors contributed equally to this work

Dr. K. AlKurdi, Dr. Dr. A. L. Jones, Prof. J. R. Reynolds, Dr. S. Barlow, and Prof. S. R. Marder

School of Chemistry and Biochemistry, Georgia Institute of Technology, Atlanta, GA, 30332, USA.

S. A. Gregory, A. Atassi, J. Rinehart, Prof. J. R. Reynolds, and Prof. S. R. Marder

School of Materials Science and Engineering, Georgia Institute of Technology, Atlanta, GA, 30332, USA.

Dr. M.P. Gordon

Applied Science and Technology Graduate Group, University of California, Berkeley, California, 94720, USA

Dr. M.P. Gordon, Prof. J.J. Urban

The Molecular Foundry, Lawrence Berkeley National Laboratory, Berkeley, California 94720, USA

Dr. J. F. Ponder Jr., and Prof. S. K. Yee

George W. Woodruff School of Mechanical Engineering, Georgia Institute of Technology, Atlanta, GA, 30332, USA.

[*] Corresponding Authors

Keywords: redox doping, charge transport, electrical conductivity, anion effects

Table of Contents Image:

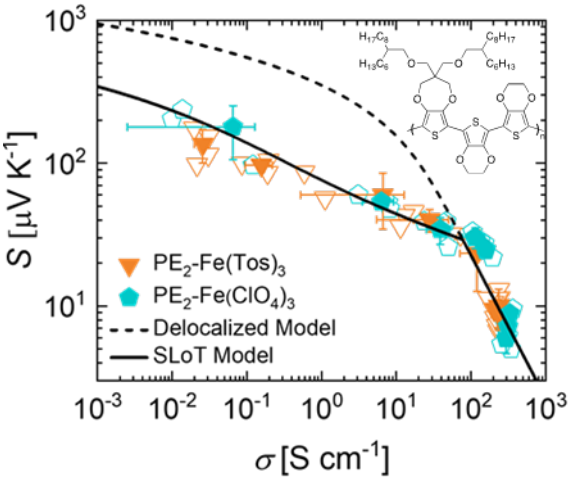

Abstract: This study investigates the charge transport properties of P3HT and poly(ProDOT-*alt*-biEDOT) (PE_2) films doped with a set of iron(III)-based dopants and as a function of dopant concentration. X-ray photoelectron spectroscopy measurements show that doping P3HT with 12 mM iron(III) solutions leads to similar extents of oxidation, independent of the dopant anion; however, the electrical conductivities and Seebeck coefficients vary significantly (5 S cm^{-1} and +82 μV K^{-1} with tosylate and 56 S cm^{-1} and +31 μV K^{-1} with perchlorate). In contrast, PE_2 thermoelectric transport properties vary less with respect to the iron(III) anion chemistry, which is attributed to PE_2 having a lower onset of oxidation than P3HT. Consequentially, PE_2 doped with 12 mM iron(III) perchlorate obtained an electrical conductivity of 315 S cm^{-1} and a Seebeck coefficient of +7 μV K^{-1}. Modeling these thermoelectric properties with the semi-localized transport (SLoT) model suggests that tosylate doped P3HT remains mostly in the localized transport regime, attributed to more disorder in microstructure. In contrast perchlorate doped P3HT and PE_2 films exhibit thermally deactivated electrical conductivities and metal-like transport at high doping levels over limited temperature ranges. Finally, the SLoT model suggests that PE_2 has the potential to be more electrically conductive than P3HT due to PE_2's ability to achieve higher extents of oxidation and larger shifts in the reduced Fermi energy levels.

1. Introduction

Doped conjugated polymers are used in a range of applications including photovoltaics,[1-3] (electrochemical)transistors,[4-6] thermoelectrics,[7] electrochromics,[8, 9] and supercapacitors.[10] Systematically evaluating polymer and dopant chemistries is a means to obtain desired electronic properties for each application. Poly(thiophene) derivatives, such as poly(3-alkylthiophenes) (P3ATs), poly(3,4-ethylenedioxythiophene) (PEDOT), and poly[2,5-bis(3-alkylthiophen-2-yl)thieno[3,2-b]thiophene] (PBTTT), and derivatives of these basic structures, receive considerable attention because of their tunable properties and high electrical conductivity when heavily doped (*i.e.* from 10^2 to 10^5 S cm^{-1}).[11, 12] Several studies have evaluated the transport in doped P3AT,[13-15] PBTTT,[16-18] and PEDOT derivatives,[5, 12] but more research is needed on soluble and solution processable dioxythiophene derivatives (XDOTs).[8, 9, 19-25] For example, recent studies have shown that these XDOTs have the ability to achieve high electrical conductivities (*ca.* 200-700 S cm^{-1}), but the precise and quantitative understanding of why certain XDOT chemistries yield higher electrical conductivities is not well understood or documented.[9, 21, 25] To better contextualize the effects of XDOT monomer selection on the resulting structural and thermoelectric properties, herein we benchmark the properties of chemically doped poly(bis(2-hexyldecyloxymethyl)propane-1,3-dioxythiophene-*alt*-bi(3,4-ethylenedioxythiophene) ((poly(ProDOT-*alt*-biEDOT), PE_2) against archetypal poly(3-hexylthiophene-2,5-diyl) (P3HT). We chose to benchmark PE_2 against P3HT (as opposed to a PEDOT derivatives) because (i) P3HT is one of the most studied conjugated polymers, (ii) P3HT and PE_2 have similar alkyl side chains and polymerization routes, and (iii) PEDOT derivatives can vary significantly depending on the polymerization technique (*e.g.* oxidative vapor, electrochemically), processing (*e.g.* dispersion with sulfonated polystyrene), and side chain chemistry (*e.g.* no side chain, hydroxyl, *etc.*). This benchmarking will serve as the quantitative basis for rationally understanding and engineering future XDOT derivatives.

Additionally, there is extensive research on the effects of dopant redox potential,[9] size,[26] mechanism,[27] and doping method[28-30] on the resulting optical and electronic properties in conjugated

polymers. The thermodynamics and kinetics of the dopant solvolysis equilibria[31-33] influences the doping processes, the residual counterion species, and the resulting electronic properties.[26, 34, 35] One of the most common *p*-type dopants is iron(III) chloride, but other iron(III) salts, such as the tosylate, triflate, and perchlorate derivatives, are possible alternatives and result in different charge balancing species being introduced into the polymer films. In the presence of relatively stronger coordinating anions (*e.g.* chloride or bromide), the iron(III) compound primarily behaves as a complex, leaving a $Fe_xX_y^-$ (termed a ferrate complex anion) as the charge balancing anion following polymer doping.[36] In contrast, when weakly or non-coordinating anion ligands are present, some solvents may substitute nearly all of the ligands around the iron center to yield a solvent-separated ion pair, leaving only X^- species as the charge balancing anions.[31-33, 37] The thermodynamics and kinetics of the solvolysis equilibria[31-33] influences the doping processes, counterion species in the doped polymer film, and the resulting electronic properties.[26, 34, 35] Some studies have examined the effects of counterion species on the resulting transport properties,[26, 29, 34, 38] but the prevailing structure-property relationships are not clear as doping thermodynamics, kinetics, and spatial incorporation convolute these relationships.

Polymer-dopant and polymer-counterion interactions affect optical and electronic transport properties. Quantifying these properties in the context of a charge-transport model can lead to deeper physical insights. Despite their utility, selecting a charge transport model consistent with a polymer-dopant-processing system is non-trivial because charge transport in polymers is sensitive to carrier density, electrostatic interactions, and structural order, all of which vary as a function of doping.[34, 35] Previous studies have utilized either localized (hopping-like) and delocalized (metal-like) transport models, but charge transport lies on a spectrum.[39] Therefore, using a semi-localized transport model (SLoT), which spans this spectrum, one can quantitively compare the underlying transport parameters and make conclusions regarding the potential for a given polymer-dopant system to achieve the desired electronic properties.[40]

Herein, we report on the chemical, structural, and charge transport properties of poly(3-hexylthiophene-2,5-diyl) (P3HT) sequentially doped with solutions of iron(III) salts at varying molarities

and counterions, and we use these P3HT properties to benchmark the properties of poly(bis(2-hexyldecyloxymethyl)propane-1,3-dioxythiophene-*alt*-bi(3,4-ethylenedioxythiophene) ((poly(ProDOT-*alt*-biEDOT), PE_2) (**Figure 1**).[21, 22] Using x-ray photoelectron spectroscopy (XPS) we measure the extent of oxidation and calculate the quantity of (bi)polaronic charge carriers (**Figure 1**), and corroborate these calculations with self-consistent thermoelectric transport and optical absorbance spectroscopy measurements. Furthermore, using grazing incidence wide angle x-ray scattering (GIWAXS) measurements, we quantify the impact of dopant counterion on microstructure. In P3HT, the extent of oxidation is weakly dependent on the dopant counterion chemistry, but the dopant counterion chemistry strongly affects the final microstructure and resulting thermoelectric properties. In PE_2, the final microstructures and resulting thermoelectric properties are not as sensitive to the specific salt used, and ultimately PE_2 achieves *ca.* 3-6 times higher electrical conductivities than P3HT. Using the SLoT model in conjunction with additional characterization methods, we conclude that PE_2 can be more electrically conductive than P3HT as it achieves higher extents of oxidation, which enables both a greater decay in charge carrier localization, and a greater increase in the reduced Fermi energy level.

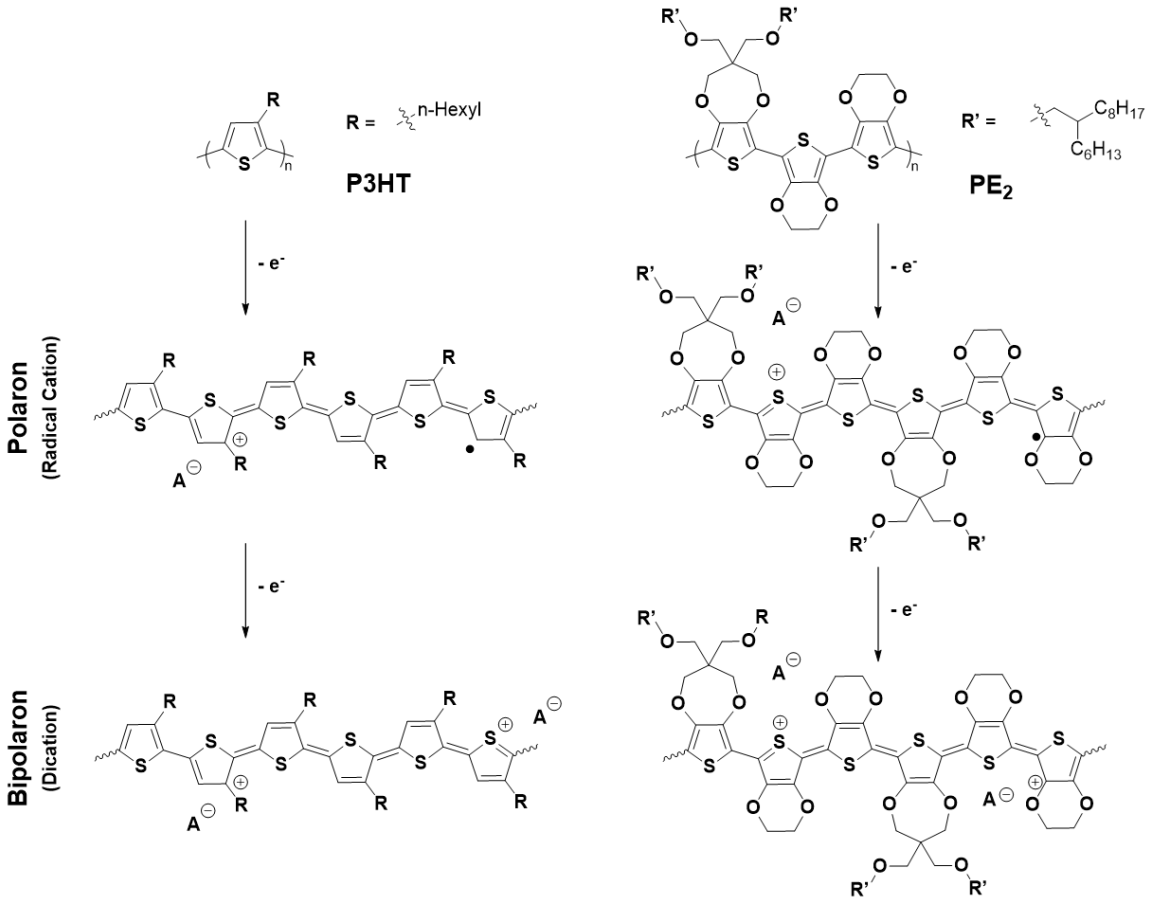

Figure 1. Doping reactions of P3HT and PE_2. P3HT and PE_2 are both susceptible to oxidative doping, where electrons are removed from the conjugated backbone. Oxidative doping leads to the formation of positively charged polaronic carriers. Depending on the extent of doping and the chemistries present, polaron charge carriers (radical cations) can spin pair to form bipolaronic charge carriers (dications). Polaronic charge carriers are also electrostatically attracted to the counter anion (A^-), whose chemical identity is a function of the polymer and dopant chemistries.

2. Results and Discussion

2.1 Experimental Approach

Our approach to quantifying the effects of dopant counterion-polymer combination on the doping process and resulting transport properties consists of three steps. First, spectroscopic and thermoelectric measurements were performed on P3HT sequentially doped at a fixed concentration (12 mM), but with varying iron(III) salts, FeX_3, for X = -Cl^-, -Br^-, -$CF_3SO_3^-$ (OTf), -$CH_3C_6H_4SO_3^-$ (Tos), and -ClO_4. These polymer and dopant chemistries were chosen because of their prevalence in the literature and commercial availability. Second, $Fe(Tos)_3$ and $Fe(ClO_4)_3$ dopants were selected for extensive evaluation because they produced the highest and lowest electrical conductivities and Seebeck coefficients in the first step. We performed detailed UV-vis-NIR, XPS, GIWAXS, and thermoelectric measurements on P3HT films sequentially doped over a wide ferric solution concentration range (which results in a sufficiently wide range of carrier densities). Similar experiments using $Fe(Tos)_3$ and $Fe(ClO_4)_3$ were performed on PE_2, and this comparison examines to what extent polymer ordering and oxidation potential may affect doping and transport properties. Third, the transport properties for all four P3HT and PE_2 polymer-dopant combinations were analyzed using the SLoT model. The fundamental transport parameters extracted from the SLoT model were then related to the chemical and structural properties. Finally, we note that the naming system used in this study consists of the polymer name followed by the corresponding iron(III)-based dopant (*e.g.* P3HT-$Fe(Tos)_3$). We use this naming system because we find that the counterion chemistry and the resulting polymer molecular structure is dependent on the chemistry and coordination environment of the iron dopant. The naming system used herein is slightly different than historical precedents. Oftentimes (electro)chemical doping reports use only the counterion species in the naming (*e.g.* P3HT-Tos), but these precedents usually do not report a complex counterion species and/or molecular changes to the monomer chemistry.[41]

2.2 Initial survey on the effects of various iron (III) dopants on P3HT thermoelectrical properties

Dopant counterions affect the doping kinetics, thermodynamics, and charge transport properties.[26, 29] Isolating the counterions' role in each of these processes is difficult because the observable properties result from their convolution. To quantify the role of the dopant counterion, five iron(III) compounds were screened, and the resulting carrier density, electrical conductivity, and Seebeck coefficient were measured. For an initial evaluation, commercially available P3HT was used (**Figures S1-S3** show the P3HT gel permeation chromatography trace, cyclic voltammogram and ^{1}H- nuclear magnetic resonance spectrogram characterizations.)). P3HT thin-films were sequentially doped by drop casting 12 mM acetonitrile solutions of iron(III) chloride, bromide, triflate, tosylate, and perchlorate on top of the films and allowing the dopant to penetrate the film, as illustrated in **Figure S4** and demonstrated in previous studies.[42] **Table S1** shows that these counterions have different volumes and coordination ability; therefore, they likely have different effects on the residual anions and resulting transport properties.

First, we examine the electrical conductivity and Seebeck coefficient of P3HT films. In general, as the extent of doping increases, the carrier density increases, and the electrical conductivity increases as the Seebeck coefficient decreases.[7] **Figure 2a** shows the electrical conductivities of P3HT films sequentially doped with 12 mM solutions of various iron(III) salts. P3HT doped with $Fe(ClO_4)_3$ is the most electrically conductive (56 S cm^{-1}) whereas the P3HT films doped with $Fe(Tos)_3$ are the least electrically conductive (5 S cm^{-1}). Consistent with this trend, **Figure 2b** shows that $Fe(ClO_4)_3$-doped films have the lowest Seebeck coefficients (+31 μV K^{-1}), whereas $Fe(Tos)_3$-doped films have the highest Seebeck coefficients (+82 μV K^{-1}). These trends in thermoelectric properties are commensurate with the optical absorbance spectra shown in **Figure S5,** which also show that P3HT-$Fe(ClO_4)_3$ has stronger polaronic absorbances than P3HT-$Fe(Tos)_3$. Therefore, these electrical conductivities, Seebeck coefficients, and optical absorbances are consistent, and together suggest that P3HT-$Fe(ClO_4)_3$ has a greater carrier density than P3HT-$Fe(Tos)_3$. We also note that these observations are consistent with a similar comparison of P3HT doping by $FeCl_3$, $Fe(OTf)_3$, and $Fe(Tos)_3$ reported by Wu *et al*.[38]

To directly quantify the extent of doping and carrier density, we used XPS. Measurements of S-2p spectra were deconvoluted and used to calculate the ratio of polaronic sulfur signals to total sulfur signal,[1, 43, 44] which is indicative of the extent of oxidation and carrier ratio (*c*).[13] This carrier ratio is used to calculated the carrier density (*n*).[20, 23, 40] Although UV-Vis-NIR and thermoelectric measurements indirectly suggest that P3HT-$Fe(ClO_4)_3$ may have more charge carriers than P3HT-$Fe(Tos)_3$ when sequentially doped with 12 mM solutions, XPS calculated carrier ratios actually show that the carrier ratios are within error for these two salts. These comparable carrier ratios indicate that these ferric dopants have comparable doping efficacies with these experimental procedures, which is reasonable considering that these salts having comparable reduction potentials.[45, 46] Furthermore, **Figure S6** shows that the carrier ratio for this series of salts varies little, with carrier ratios of *ca.* 0.22-0.30 (corresponding to 1 carrier for every ~4 thiophene rings) independent of the ferric dopant. Although the carrier ratios are comparable, there are several differences amongst these dopant systems. FTIR measurements in **Figures S7-10** show that P3HT films doped with $Fe(ClO_4)_3$ uniquely exhibit thiophene oxide formation.[47] **Table S2** shows that iron was not detected by XPS in films doped with $Fe(ClO_4)_3$ and $Fe(OTf)_3$, likely because both salts contain weakly coordinating anions. In contrast, some iron was detected in all the other films, up to a maximum of 8 atomic percent with $FeCl_3$; $FeCl_3$ having the most residual iron is consistent with Cl being the most strongly coordinating counterion in this study (**Table S1**) and is consistent with previous reports.[40] Finally, **Table S1** shows that counterion sizes vary substantially, and the largest difference is between tosylate anions and chloride anions (154 *vs.* 66 $Å^3$).

It is fully expected that the above listed differences affect the electrical conductivity and Seebeck coefficients, and this is especially apparent between P3HT-$Fe(Tos)_3$ and P3HT-$Fe(ClO_4)_3$. These two systems have approximately an 11 and 3 times difference in electrical conductivity and Seebeck coefficient, respectively, that cannot be explained solely by the small differences in carrier ratios (carrier densities) nor solely with delocalized transport models.[40, 48, 49] Therefore, it is important to acknowledge that the varying

dopant counterion coordination ability, counterion size, and polymer-counterion interactions all affect optical and charge transport properties[48, 50, 51] and requires further investigation.

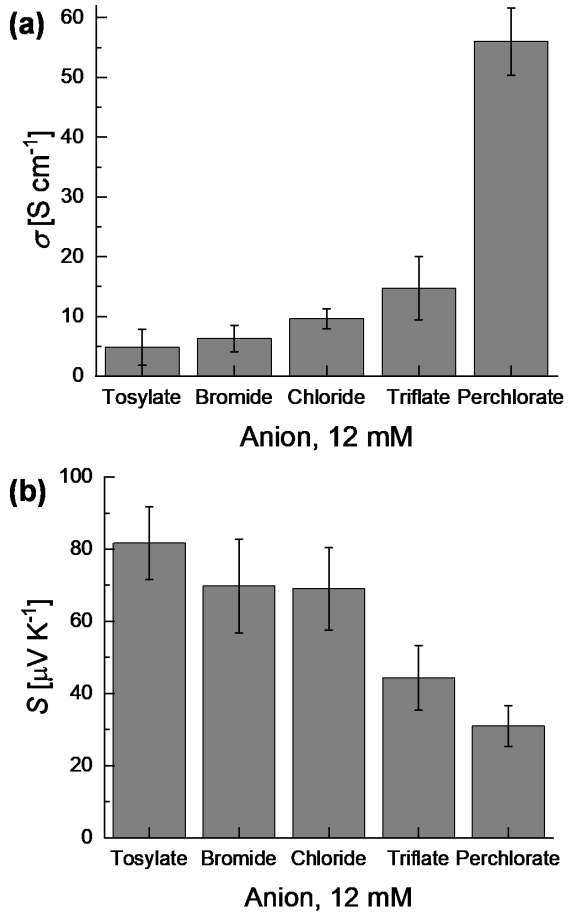

Figure 2. Survey thermoelectric properties of P3HT films sequentially doped with 12 mM solutions of different iron(III) salts in acetonitrile. (a) Electrical conductivity and (b) Seebeck coefficients averaged over at least 3 separate films, with error bars representing sample-to-sample standard deviation.

2.3 Spectroscopic analysis of P3HT and PE_2 doped with $Fe(Tos)_3$ and $Fe(ClO_4)_3$

To quantify to what extent counterion identity and concentration affect transport properties, we sequentially doped P3HT with $Fe(Tos)_3$ and $Fe(ClO_4)_3$ over a wide range of solution concentration, 1.5 to 100 mM. Additionally, we sequentially doped PE_2 with $Fe(Tos)_3$ and $Fe(ClO_4)_3$ solutions with concentrations ranging from 0.1 to 12 mM. Offset doping concentration ranges were used because P3HT and PE_2 have different doping susceptibilities and electrical conductivities, and our instrumentation necessitates sheet resistances less than *ca.* 10 MΩ for reportable thermoelectric measurements. Additionally, this offset doping range is needed for us to capture a sufficiently large range of S, σ values to use the SLoT model for these polymers. Furthermore, the SLoT model uses carrier ratio (carrier density) as the independent variable, and not dopant solution concentration, so this dopant solution concentration offset does not impede our primary goal of quantifying the interrelationships between chemical structure, microstructure, and charge transport properties.

The extent of doping was first qualified with UV-Vis-NIR spectroscopy (**Figure S11**). **Figure S11** shows that with increasing solution concentration, polaronic absorption in the mid-infrared (MIR) increases and neutral absorption in the visible decreases, and this is indicative of increasing extent of oxidation. Additionally, these spectra show that PE_2 is more susceptible (*i.e.*, is oxidized to the same extent at lower dopant molarities) to doping than P3HT. Explicitly, PE_2 pristine π-π^* absorbances bleach near 3 mM $Fe(Tos)_3$ or $Fe(ClO_4)_3$ and remains bleached through 12 mM. In contrast, P3HT pristine π-π^* bleaching requires at least 25 mM $Fe(ClO_4)_3$, and $Fe(Tos)_3$ cannot effectively bleach the pristine π-π^* peak. The ability of less concentrated solutions to bleach the pristine π-π* absorption of PE_2 is consistent with its lower oxidation potential (onsets of oxidation are 0.3 V and -0.7 V vs. ferrocene for P3HT and PE_2).[21, 38]

To quantify the carrier ratio and the doping mechanisms in P3HT and PE_2 films, we used XPS. **Figure 3a-c** shows representative deconvoluted spectra for pristine and 12 mM doped P3HT films, and **Figure 3d-f** shows similar spectra for PE_2 films. For the P3HT spectra (**Figure 3a-c)**, pristine and neutral thiophene peaks occur between *ca.* 163 and 164.5 eV, polaronic thiophene peaks (polaronic charge carriers)

occur between *ca.* 164.5 and 166 eV, and S=O peaks (from tosylate or sulfones) occur between *ca.* 167 and 170 eV. Notably, doping with $Fe(ClO_4)_3$ yields sulfur with binding energies at *ca.* 167 eV, consistent with chemically oxidizing thiophenes to thiophene oxides; this observation is further confirmed with FTIR measurements, has been previously reported in literature, and is discussed in detail in **Note S3**. [47, 52] To approximate the carrier ratio, the thiophene S-2p feature was deconvoluted into neutral sulfur contributions and polaronic sulfur (denoted as S*) contributions. The ratio of the S* peak area to the total thiophene (and thiophene oxide, where applicable) peak area is assumed to be equal to the number of holes per thiophene unit, which is equal to the carrier ratio.[1, 43, 44, 53] Although a single polaronic cation charge carrier is likely delocalized over multiple thiophene moieties, XPS can be used to quantify the average extent of oxidation and carrier ratio. For example, the carrier ratio for P3HT calculated from rigorously deconvoluted XPS S-2p spectra using a single neutral doublet and a single oxidized doublet is consistent with P3HT carrier ratios measured using cyclic voltammetry.[43] Additionally, for $Fe(Tos)_3$-doped films, the extent of oxidation was also quantified using the abundance ratio of tosylate counterions (using the sulfoxide doublet at *ca*. 168 eV for $Fe(Tos)_3$ doped films) with respect to thiophene, which is commonly employed in the PEDOT literature.[12] Finally, for P3HT-$Fe(ClO_4)_3$ films, the extent of oxidation was also calculated by deconvoluting the C-1s spectra (**Note S3**). The pristine sp^3 and sp^2 carbon are convoluted near *ca.* 284.6 eV, but as the doping level increases a new peak 286.2 eV emerges, increases, and is attributed to oxidized aromatic carbons.[54, 55]

The PE_2 XPS spectra (**Figure 3d-f**) show similar features to the P3HT spectra, but the doped PE_2 films show additional features at binding energies between 166 and 167.5 eV (denoted S** in **Figure 3**). Previous works on PEDOT and P3HT have attributed the S-2p energies near 166 eV to multi-polaronic charge carriers, but the exact assignment is not clear.[1, 44, 56-58] For example, Wegner *et al.* correlated the presence of higher binding energies in P3HT doped with borate salts with EPR measurements, and they assigned features at *ca.* 166 eV to bipolaron formation.[14] Similarly, Marrikar *et al*. assigned binding energies near 166-168 eV to heterogeneously doped and oxidized regions in PEDOT films.[53] In contrast, in

PEDOT systems this additional peak area may be ascribed to asymmetric scattering of the ejected photoelectrons by the more delocalized valence band.[12, 54, 56] Ultimately, we recognize that there is uncertainty regarding this peak, but here we ascribe the peaks near 166 eV in PE_2 to polaronic charge carriers (S^{**} in **Figure 3**). Finally, we note that pristine PE_2 is susceptible to air oxidation; air oxidation of the pristine may be responsible for some peaks intensities at higher binding energies in **Figure 3d** at 166 eV. This air doping can result in electrically conductive PE_2 thin-films (*ca*. 15 S cm^{-1} at 35 nm)[21] and is notably evident in the S-2p spectra because XPS is a surface sensitive technique; however, thicker PE_2 films show lower electrical conductivities (*ca.* 10^{-4} S cm^{-1} at 150 nm),[21] and the pristine PE_2 films in this study are even thicker (*ca.* 700 nm thick) and are electrically insulating (< 10^{-4} S cm^{-1}), suggesting the PE_2 films in this study are not substantially air doped.

Now that we deconvoluted and quantified the XPS spectra for P3HT and PE_2 at 12 mM, we turn to quantifying these changes at each doping level. For each polymer-dopant chemistry-dopant molarity combination, we calculate the carrier ratio and the extent of thiophene oxide formation. The carrier ratio is quantified using the previously described three methods: (1) the ratio of S* and S** (polaronic, oxidized thiophenes) abundance to total thiophene abundance, (2) the ratio of tosylate abundance to total thiophene abundance, and (3) the ratio of oxidized aromatic carbons to aromatic carbons.

For P3HT **(Figure 4a**), as the solution concentration increases, the extent of doping and the (bi)polaronic abundance increases. Specifically, at high doping levels (> 25 mM), the average extent of doping (from all deconvolution methods) and carrier ratio begins to saturate at *ca*. 0.35, corresponding to one charge carrier for every three rings. These carrier ratio trends and values are consistent with previously reported spectroscopic and electrochemical P3HT doping studies and are consistent with the trends in optical (**Figure S11**) and thermoelectric measurements (*vide infra*) presented herein.[6, 43, 59] Additionally, **Figure 4a** shows that at most dopant concentrations, P3HT films doped by $Fe(Tos)_3$ or $Fe(ClO_4)_3$ have similar carrier ratios (within error), consistent with the initial analysis in **Figure 2** and **Figure S6**.Finally,

in the case of $Fe(ClO_4)_3$-doped P3HT- films, there is an increasing amount of chemically oxidized sulfoxide rings present, reaching a maximum near 35%.

Like P3HT, **Figure 4b** shows that with increasing solution molarity, the PE_2 films become increasingly doped; however, doping saturates at a greater carrier ratio of *ca.* 0.5, or one charge carrier per two thiophene rings. This carrier ratio is consistent with previous PEDOT reports,[5, 12, 58] and this larger maximum carrier ratio ($c_{\max}$) may be because PE_2 is more electron rich and easily oxidized; this is consistent with previous reports that show increasing the electron-richness of thiophene derivatives increases their carrier density (extent of oxidation, carrier ratio) and their electrical conductivity when comparably doped.[23, 60, 61] In contrast, the thiophenes in PE_2 are less susceptible to chemical oxidation to sulfoxide by $Fe(ClO_4)_3$ than P3HT, reaching a maximum level of *ca.* 10% *vs.* 35%. We speculate that the non-bonding S—O interactions in the PE_2 backbone act as a kinetic barrier to chemical oxidation; the O atoms shield the adjacent S atoms, both sterically and electronically, due to the O lone pair interaction and the resulting proximity to the S atoms.[62] Additionally, PE_2's higher carrier ratios relative to P3HT may also hinder oxygen-transfer oxidation since the increased positive charge per thiophene ring may make the sulfur more difficult to chemically oxidize. Similar to P3HT, doping PE_2 with either $Fe(Tos)_3$ or $Fe(ClO_4)_3$ result in roughly the same carrier ratio at a fixed solution molarity. These PE_2 carrier ratio trends and values are consistent with the trends in optical (**Figure S11**) and thermoelectric measurements (*vide infra*) presented herein.. Finally, we note that at a comparable extent of doping and carrier density, polymer-dopant systems may show different optical and transport properties. These differences in properties may be attributed to differences in extinction coefficients, carrier mobilities, and/or effective masses, which must further contextualized and confirmed using additional microstructural and charge transport measurements.[48, 51]

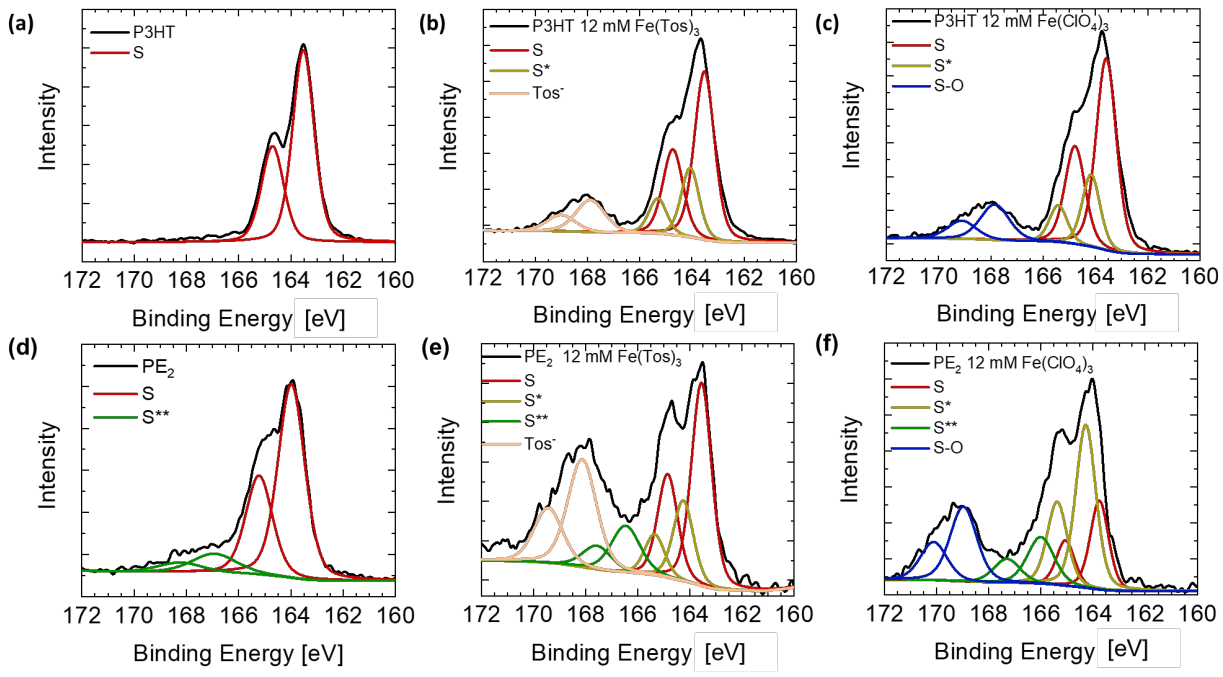

Figure 3. Representative XPS S 2p spectra for P3HT and PE_2. (a) pristine P3HT. (b) P3HT doped with 12 mM $Fe(Tos)_3$. (c) P3HT doped with 12 mM $Fe(ClO_4)_3$. (d) pristine PE_2. (e) PE_2 doped with 12 mM $Fe(Tos)_3$. (f) PE_2 doped with 12 mM $Fe(ClO_4)_3$. Additional XPS deconvolution procedures are in Note S5. The range of binding energies used to fit specific chemical species across all polymer and dopant chemistries is quite narrow (< 0.5 eV for all thiophene species, see Figure S12,13), suggesting that all deconvoluted peaks used here are needed and repeatable.

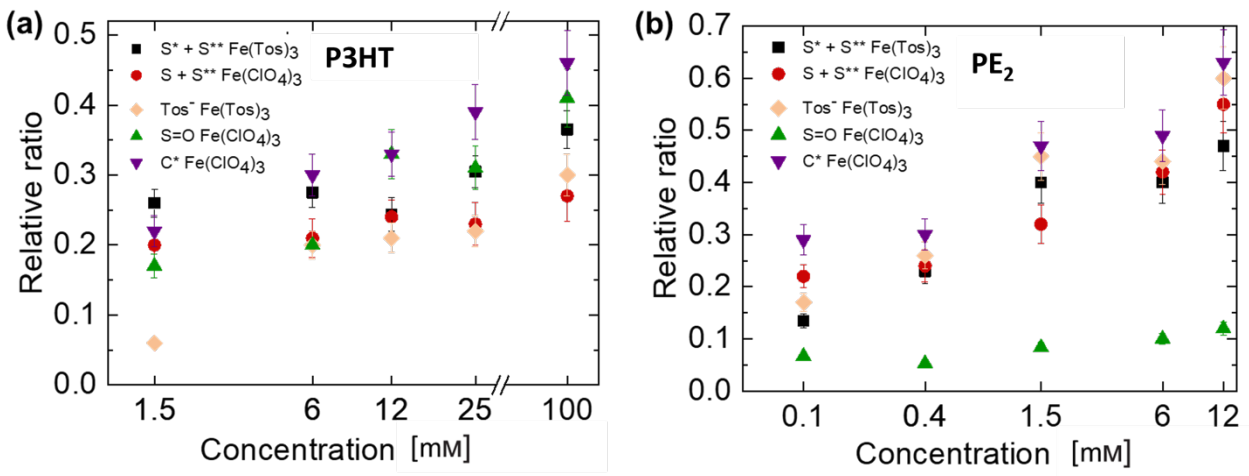

Figure 4. Relative ratios calculated from XPS spectra as a function of dopant solution concentration for (a) P3HT. (b) PE_2. The S* + S** ratio represents the charge carrier ratio, calculated from the area ratio of polaronic thiophenes to total thiophenes. The Tos^- ratio represents the charge carrier ratio, calculated from the area ratio of the tosylate signal to the total thiophene signal. The C* ratio represent the charge carrier ratio, calculated from the area ratio of oxidized aromatic carbon to total aromatic carbon from the C-1s spectra. S=O ratio represents the area ratio of thiophene oxides to total thiophene rings in films doped with $Fe(ClO_4)_3$.Note that data is presented on a logarithmic horizontal axis for clarity.

2.4 Structural analysis of P3HT and PE_2 doped with $Fe(Tos)_3$ and $Fe(ClO_4)_3$

To investigate the structural impact of doping, GIWAXS diffractograms and in-plane linecuts of pristine and increasingly doped films are examined (**Figure 5)**. **Figure 5a** shows the in-plane linecuts $Fe(ClO_4)_3$-doped P3HT films. As the doping molarity increases, the alkyl side chain packing's (100) peak shifts to smaller *q* values (larger *d* spacing in real space,)) and the π-π stacking's (010) peak shifts to larger *q* values (smaller *d* spacing in real space.)). Furthermore, the concomitant expansion of the alkyl packing and contraction of the π-π stacking suggests that ClO_4 counterions are intercalated in the side chains and not in the π-π stacks.[63] Similar trends are observed with P3HT-$Fe(Tos)_3$ (**Figure 5b**), but there are two distinct differences. First, **Tables S3,4** shows that the π-π stacking ranges from 3.51 Å to 3.54 Å in 12 mM and 100 mM P3HT-$Fe(ClO_4)_3$ films, but the π-π stacking ranges from 3.6 Å to 3.59 Å in 12 mM and 100 mM P3HT-$Fe(Tos)_3$ films. The π-π stacking distance influences molecular orbital overlap and charge carrier mobility between chains, with smaller distances yielding increased delocalization and mobility.[64] Therefore, a seemingly small difference in π-π stacking may contribute towards notably different transport properties. Second, the intensity of P3HT-$Fe(Tos)_3$ peaks is substantially reduced with respect to the P3HT-$Fe(ClO_4)_3$ peaks. The intensity of these linecuts is indicative of the doped films' propensity for ordering. Therefore, the lower peak intensities in the P3HT-$Fe(Tos)_3$ films indicates that $Fe(Tos)_3$ disrupts the ordered regions to a greater extent than $Fe(ClO_4)_3$. This is likely because the perchlorate anions are approximately half the volume of tosylate ions (which could be larger tosylate complexes due to residual Fe signal in XPS, (Table S2)),and therefore perchlorate anions disrupt the microstructure less.[38] Interestingly, the formation of thiophene oxides via perchlorate chemical oxidation does not seem to significantly alter ordering, and this could indicate that the chemical oxidation mostly occurs in amorphous regions of the films, which is not observable using GIWAXS. Overall, these observations are consistent with those reported by Wu *et al.*, who similarly found that $Fe(Tos)_3$ disrupts the P3HT microstructure to the greatest extent.[38]

Next, we turn to analyzing the structural changes in PE_2. **Figure 5c** shows the in-plane linecuts for PE_2-$Fe(ClO_4)_3$, and **Figure 5d** shows the in-plane line cuts for PE_2-$Fe(Tos)_3$. Initially, pristine PE_2 is heavily

disordered, as seen by the broad (100) peak; however, as the doping level increases, the (100) peaks become increasingly defined, and higher order (up to (400)) reflections are observed. We note that this is an exceptionally high ordered reflection for an XDOT polymer (with[8, 20, 24] or without side chains[65, 66]), and this indicates that PE_2 can achieve a comparatively high extent of ordering. Additionally, the (100) peak narrows and shifts to lower q values with increasing doping. These trends indicate that the crystallite size increases, the lamellar spacing increases, and that the dopant counterions likely incorporate in the alkyl region. Notably, in both P3HT and PE_2 the alkyl side chains expand and the $\pi - \pi$ stack with increased doping level, and this suggests that doping occurs via integer charge transfer and not via charge transfer complex formation.[30, 63, 67] Ultimately, these trends suggests that doping increases the extent of ordering in PE_2, which contrasts the observations of P3HT reported herein and of other doping studies.[23, 27, 67]

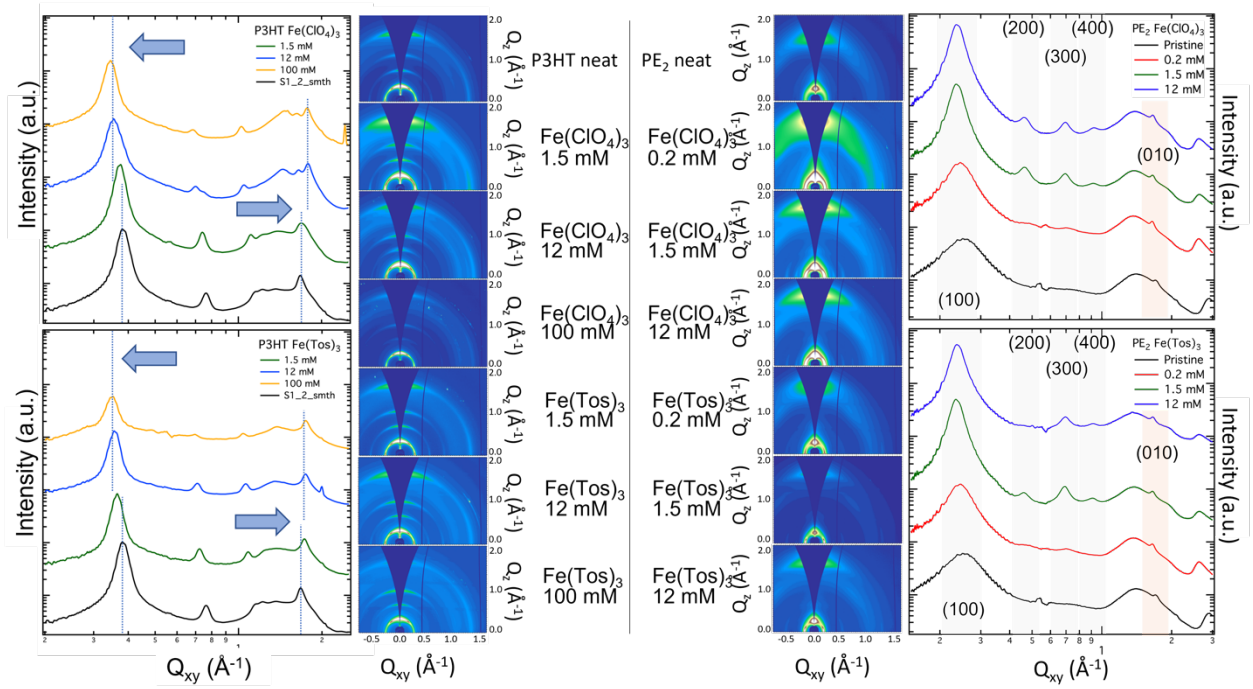

Figure 5. GIWAXS in-plane linecuts and diffractograms for P3HT and PE_2 films sequentially doped with $Fe(Tos)_3$ and $Fe(ClO_4)_3$ at varying solution molarities. (a) P3HT-$Fe(ClO_4)_3$. (b) P3HT-$Fe(Tos)_3$. In these linecuts, the blue arrows and vertical dashed lines help guide the eye to show the general trends for the (100) peaks and π-π peaks. Note that the P3HT diffractograms are located left of center and range from 1.5 to 100 mM. (c) PE_2-$Fe(ClO_4)_3$. (d) PE_2-$Fe(Tos)_3$. The peaks in PE_2 are broader and less commonly reported, so individual diffraction peaks are labeled and highlighted. Note that PE_2 diffractograms are located right of center and range from 0.2 to 12 mM. **Figures S20,S21** show nearly out-of-plane linecuts, and **Table S3, S4** tabulate *d*-spacings.

2.5 Effect of dopant selection on P3HT and PE_2 transport parameters, analyzed through the SLoT model

In the previous sections, we showed that P3HT and PE_2 polymers doped with $Fe(Tos)_3$ and $Fe(ClO_4)_3$ have distinct chemical and structural differences. These differences likely affect the resulting transport properties. Therefore, we succinctly highlight the most notable five differences before using the SLoT analysis to quantify how these differences affect measurable transport properties. (1) PE_2 is more electron rich and likely has more delocalized charge carriers than P3HT because PE_2 has dioxy- donating groups that promote a more quinoid-like structure;[9] electrochemical and spectroscopic measurements suggest that these donating groups increase doping susceptibility and the maximum extent of oxidation (maximum carrier ratio). (2) XPS measurements and deconvolutions show that at a fixed solution concentration of $Fe(ClO_4)_3$ and $Fe(Tos)_3$ yield a comparable number of polaronic charge carriers. (3) Furthermore, $Fe(ClO_4)_3$ can chemically oxidize to yield thiophene oxides; this chemical oxidation is more prominent in P3HT than in PE_2. (4) GIWAXS measurements show that pristine P3HT is more ordered than PE_2, but P3HT ordering decreases with increased doping level while PE_2 ordering increases with increased doping level. (5) Additionally, doping with $Fe(Tos)_3$ disrupts the ordering in P3HT to a greater extent than doping with $Fe(ClO_4)_3$, likely because of the difference in counterion sizes, but there is not an observable difference with PE_2.

To quantify how the structural and chemical differences between P3HT and PE_2 doped with $Fe(Tos)_3$ and $Fe(ClO_4)_3$ affect charge transport, temperature dependent Seebeck coefficients, electrical conductivities, and carrier ratios were analyzed within the SLoT model.[40] The SLoT model uses a Boltzmann transport formalism with a semi-localized transport function (σ_E) to isolate hopping-like and metal-like contributions to the observable S and σ, and the SLoT model quantifies how these contributions vary with respect to carrier ratio (c). The SLoT model transport function is,

$$\sigma_{\mathrm{E}}(E,T,c) = \begin{Bmatrix} 0,\ E < E_{\mathrm{t}} \\ \sigma_0 \exp\left(-\frac{W_H(c)}{k_B T}\right) \times \left(\frac{E-E_{\mathrm{t}}}{k_{\mathrm{B}} T}\right),\ E \geq E_{\mathrm{t}} \end{Bmatrix}. \quad (1)$$

Therefore, the resulting expressions for the electrical conductivity and Seebeck coefficient, are

$$\sigma = \sigma_0 \exp\left(-\frac{W_H(c)}{k_B T}\right) \times \int_0^{+\infty} \left(\frac{E-E_{\mathrm{t}}}{k_{\mathrm{B}} T}\right)\left(-\frac{df}{dE}\right) dE \quad (2)$$

and

$$S = \left(\frac{k_{\mathrm{B}}}{e}\right) \times \frac{\int_0^{+\infty}\left(\frac{E-E_{\mathrm{t}}}{k_{\mathrm{B}} T}\right)\left(\frac{E-E_{\mathrm{t}}}{k_{\mathrm{B}} T}-\frac{E_{\mathrm{F}}-E_{\mathrm{t}}}{k_{\mathrm{B}} T}\right)\left(-\frac{df}{dE}\right)dE}{\int_0^{+\infty}\left(\frac{E-E_{\mathrm{t}}}{k_{\mathrm{B}} T}\right)\left(-\frac{df}{dE}\right)dE}. \quad (3)$$

Eq. 1 shows that charge carriers with energies (E) located below the transport edge (E_{t}) do not contribute to charge transport. Evaluating Eq. 1 within the Boltzmann transport integrals enables a mathematical convenience, where this transport edge can be used as the zero-energy reference level and lower integral bound for Eq. 2 and Eq. 3.[49] In contrast, charge carriers with $E \geq E_{\mathrm{t}}$ contribute to transport, and their contribution is weighted by $\sigma_0 \exp\left(-\frac{W_H(c)}{k_B T}\right)\left(\frac{E-E_{\mathrm{t}}}{k_{\mathrm{B}} T}\right)$. σ_0 is the SLoT transport function prefactor. σ_0 has units of S cm^{-1}, is independent of doping level and carrier density, and laterally shifts the $S(\sigma)$ curve. In ideal systems, σ_0 can be related to electron energy independent parameters, such as the curvature of the density of electronic states,[48] and systems with larger σ_0 values typically exhibit larger electrical conductivities (Eq. 2). $\exp\left(-\frac{W_H(c)}{k_B T}\right)$ captures localized contributions to the observable transport properties. W_{H} is the localization energy and captures charge carrier localization due to polaronic effects, disorder, and electrostatic interactions, akin to localized transport formalisms like the Mott polaron model and Marcus theory. This localization precludes metal-like transport, but localization generally decreases in magnitude as the carrier ratio increases, as calculated using XPS. Additionally, as W_{H} decreases, σ increases, and σ becomes less thermally activated. $\left(\frac{E-E_{\mathrm{t}}}{k_{\mathrm{B}} T}\right)$ is electron-energy dependent contribution to transport and is akin to the transport models used for crystalline inorganic semiconductors.[48, 49] As the extent of doping increases and Fermi energy level increases with respect to the transport edge, charge carriers

occupy increasingly higher electronic states with respect to the transport edge and contribute more to charge transport. Additionally, as the extent of doping increases, the Fermi energy increases with respect to the transport edge, denoted by $\eta = \frac{E_F - E_t}{k_B T}$, the electrical conductivity increases, and the Seebeck coefficient decreases (Eq. 3). Notably at 300 K, even if the Fermi energy level is below the transport edge ($E_F < E_t, \eta < 0$) with a distribution and population of carriers whose energies are less than the transport edge and do not contribute to transport, there will be a distribution and population of carriers that have energies greater than the transport edge and meaningfully contribute to charge transport carriers (as governed by the Fermi-Dirac distribution and density of electronic states). Eq. 3 also shows that the Seebeck coefficient is independent of $\sigma_0 \exp\left(-\frac{W_H(c)}{k_B T}\right)$ and that the Seebeck is only a function of η. Lastly, note that $\left(-\frac{df}{dE}\right)$ is the first derivative of the Fermi-Dirac distribution with respect to energy, also known as the selection function, and weighs charge carriers' contributions to the observable transport properties. Ultimately, all parameters in the SLoT model are experimentally measurable and calculable, and we can quantify fundamental transport relationships such as, how quickly does localization decrease with increasing carrier ratio ($W_H(c)$), how quickly do the electron states become populated with charge carriers with increase carrier ratio ($\eta(c)$), and the characteristic σ_0 that is constant for a polymer-dopant system.

First, we examine the $\eta(c)$ relationship. **Figure 6a** and **Figure 6d** plot the $\eta(c)$ for P3HT and PE_2, respectively, as a function of carrier ratio; η values were calculated from Seebeck coefficient measurements using Eq. 1 and Eq. 3, and carrier ratios were calculated from XPS deconvolutions (**Figure 3,4, S11-17, SLoT Model-P3HT and PE2 Study.xlsx**). These $\eta(c)$ curves are significantly different, suggesting that dopant and polymer chemistry affect the distribution and filling of electronic states. The x-intercept in an $\eta(c)$ plot is the charge carrier ratio (c_t) needed for the for the Fermi energy level to exceed the transport edge and captures the onset of appreciable charge transport. **Table 1** shows that c_t for P3HT-$Fe(Tos)_3$ is 0.02, which is similar to c_t for P3HT-$FeCl_3$ and P3HT-$NOPF_6$,[13, 40] but c_t is 0.18 for P3HT-$Fe(ClO_4)_3$. This large c_t for P3HT-$Fe(ClO_4)_3$ is similar to those for PE_2 and PEDOT[5, 12, 40] and indicates that these systems

need to be heavily oxidized to achieve appreciable thermoelectric properties. Interestingly however, P3HT-Fe(ClO_4)$_3$ has a steeper slope in comparison to P3HT-Fe(Tos)$_3$ and obtains higher η values. Notably, at similar charge carrier ratios (*ca*. 0.33), η is *ca*. 6 and 14 for P3HT-Fe(Tos)$_3$ and P3HT-Fe(ClO_4)$_3$, respectively. At this equivalent carrier ratio, P3HT-Fe(ClO_4)$_3$ has a higher η value, which is consistent with its higher electrical conductivities and mobilities (**Figures 2, 6c, S23**). P3HT-Fe(ClO_4)$_3$ may obtain higher η values because thiophene oxide formation alters the thiophene ring planarity and intra-ring aromaticity,[68] thereby promoting charge carrier delocalization inter-ring. Increased charge carrier delocalization is oftentimes concomitant with an increasing electronic bandwidth,[69] which is consistent with the higher η values and lower effective masses (**Figure S23**). Additionally, at c = 0.33 PE_2, doped with either chemistry, obtains η values comparable to P3HT-Fe(ClO_4)$_3$; however, PE_2 can obtain higher extents of oxidation, up to c ~ 0.5, likely because of its increased electron-richness. Furthermore, the oxygen lone pairs in EDOT can also participate in π-donation into the thiophene ring and thereby promote a quinoid structure and charge carrier delocalization inter-ring as well. For PE_2, as c continues to increase beyond 0.33 to 0.5 (a 50% increase), η triples to *ca.* ~42, which also triples σ.

Second, we turn to examining the $W_{\mathrm{H}}(c)$ relationships. **Figures 6b** and **Figure 6e** plot the $W_{\mathrm{H}}(c)$ for P3HT and PE_2, respectively, as a function of carrier ratio, and W_{H} is calculated from temperature dependent thermoelectric measurements (Eq. 2, Eq. 3, and **Figure S22)**. These $W_{\mathrm{H}}(c)$ curves are again substantially different, suggesting that polymer chemistry (*e.g.* electron richness) and polymer ordering (*e.g.* the microstructure after doping) affect the spatial and electrostatic localization of charge carriers. **Table 1** tabulates the modeled maximum localization energy in the dilute carrier limit ($W_{\mathrm{H}}^{\mathrm{max}}$), the rate at which localization diminishes ($W_{\mathrm{H}}^{\mathrm{slope}}$), and the carrier ratio where localization is minimal (c_{d}). **Figure 6b** shows that at high carrier ratios ($c \gtrsim 0.33$), P3HT-Fe(ClO_4)$_3$ has minimal localization and achieves metal-like transport ($W_{\mathrm{H}} \lesssim 25$ meV) while P3HT-Fe(Tos)$_3$ still has substantial localization with substantial thermal activation energy (see **Figure S22** for temperature dependent plots). This trend is likely because the P3HT-Fe(Tos)$_3$ microstructure is more heavily disrupted in comparison to P3HT-Fe(ClO_4)$_3$, as seen in

the GIWAXS in **Figure 5**. Next, we turn to PE_2, which has a comparable c_d as P3HT-$Fe(ClO_4)_3$ (**Figure 6b,e).** We also note that PE_2 has a larger c_d than that for previously reported oxidatively polymerized PEDOT-$Fe(Tos)_3$ (~0.34 *vs.* 0.2).[12, 40]This difference in c_d may be due to electrically insulating side chains in PE_2, which are not found in the oxidatively polymerized PEDOT-$Fe(Tos)_3$, and we note that cleaving the side chains from XDOT derivatives can significantly enhance the electrical conductivity.[25] Additionally, heavily doped PE_2 films ($c \gtrapprox 0.35$) can exhibit thermally deactivated and metal-like $\sigma(T)$ properties over multiple doping levels (**Figure S22**). Other polymer-dopant systems exhibit metal-like $\sigma(T)$ values, but oftentimes these studies report an isolated doping level and/or do not report carrier densities;[17, 18] this report compliments previous studies by more systematically sweeping doping levels and (reduced) Fermi energy levels and quantifying the carrier ratios (densities) in the vicinity of this insulator to metal $\sigma(T)$ transition. Furthermore, this study demonstrates that increasing c_{max} and decreasing c_d is a strategy to promote metal-like electrical conductivities and mobilities. Finally, we note that the systematic decrease and eventual absence of localization in P3HT-$Fe(ClO_4)_3$ and PE_2 is concomitant with the increasing and then plateauing of drift mobilities and weighted mobilities a function of increasing c and η, as shown in **Figure S23**. Oftentimes, ideal delocalized inorganic semiconductors have a nearly constant weighted mobility as the carrier density increases, especially in comparison to drift mobilities calculated using a carrier density.[50] Therefore, the concomitant absence of localization and plateaued weighted mobility in P3HT-$Fe(ClO_4)_3$ and PE_2 is consistent with transport dominated by delocalized charge carriers.

Finally, we turn to analyzing the $S(\sigma)$ curve and σ_0. **Figure 6c** and **Figure 6f** shows the experimental $S(\sigma)$ datasets, the delocalized (metal-like) curve calculated using the Kang-Snyder $s = 1$ model,[49] and the SLoT model calculated using the $\eta(c)$ and $W_H(c)$ relationships with no freely adjustable parameters.[40] In the regime where the SLoT model is not colinear with the delocalized model curve, charge transport can be thought as dominated by localized contributions, and the electrical conductivity is systematically reduced by a factor of $\exp\left(-\frac{W_H(c)}{k_B T}\right)$. When $W_H(c) \lesssim k_B T$, localized contributions are minimal and the SLoT curve becomes colinear with a delocalized curve. The P3HT-$Fe(ClO_4)_3$ $S(\sigma)$ dataset

and SLoT curve coincide with the delocalized curve in the high doping limit, but the converse is not true for P3HT-Fe(Tos)$_3$. This is consistent with the previous localization and (weighted) mobility analysis. Additionally, the value calculated for σ_0 from the $S(\sigma)$ curve must be consistent for both the localized and delocalized regimes and be consistent with the calculated values for σ_0 from temperature dependent thermoelectric measurements (**Figure S22**). **Table 1** shows that σ_0 = 30 S cm^{-1} for P3HT-Fe(Tos)$_3$ and 7 S cm^{-1} for P3HT-Fe(ClO$_4$)$_3$. This is a significant difference, and at first, these σ_0 values may seem counterintuitive because P3HT-Fe(Tos)$_3$ is less electrically conductive than P3HT-Fe(ClO$_4$)$_3$ in the high doping limit, yet P3HT-Fe(Tos)$_3$ has the larger σ_0 value; however, recall here that σ_0 is (ideally) independent of doping level, carrier density, electron energy, and localization contributions. This difference in σ_0 is most clear when both systems have the same transport properties and parameters. For example, when $c \sim 0.2$, $\eta \sim 3$, $S \sim 85\ \mu$V K^{-1}, $W_{\mathrm{H}} \sim 85$ meV, P3HT-Fe(Tos)$_3$ has a σ of ~1.6 S cm^{-1} while P3HT-Fe(ClO$_4$)$_3$ has a σ of ~0.5 S cm^{-1} (see the gap between the SLoT models in **Figure 6c** near 1-50 S cm^{-1}).

Figure 6f shows that the SLoT model also captures the curvatures, slopes, and nominal coordinates for most PE$_2$ data points. Additionally, both PE$_2$ doped with Fe(Tos)$_3$ and Fe(ClO$_4$)$_3$ have similar curvatures, slopes, and coordinates, so the same SLoT model curve with the same SLoT transport function prefactor (σ_0 = 9 S cm^{-1}) models both data sets. Using the same SLoT model curve is consistent with the previous observations that both PE$_2$ data sets have similar $W_{\mathrm{H}}(c)$ and $\eta(c)$ curves. Despite this consistency, a shortcoming in the SLoT model for this PE$_2$ system is that the SLoT model does not as accurately capture the slope in the high-doping regime as it does for P3HT and PBTTT.[40] Explicitly, SLoT models a gradual slope in the delocalized regime in **Figure 6c, f**, but the PE$_2$ data sets arguably show a precipitous decrease in Seebeck coefficient. We believe that the highly doped PE$_2$ slope is not as accurately captured because the energy dependence of the transport function may not always be linear.[40, 49, 70] Capturing a changing energy dependence is an area of current research and may also explain the large η values.

Finally, we examine why PE$_2$ -Fe(ClO$_4$)$_3$ obtains higher σ values than P3HT-Fe(ClO$_4$)$_3$ (**Table 1**). Both P3HT and PE$_2$ exhibit increasing σ with increasing extents of oxidation, and at a common c value of

0.33, both PE_2-$Fe(ClO_4)_3$ and P3HT-$Fe(ClO_4)_3$ have comparable η values, little to no localization, similar σ_0 values, and comparable σ values near 100 S cm^{-1}. Therefore, the primary difference between these two systems is that PE_2 can obtain higher *c* values up to ~ 0.5, likely because of its increased electron richness due to the dioxy- donating groups. Therefore, consistent with the analysis in **Figure 6a, d** and parameters in **Table 1**, as *c* continues to increase from 0.33 to 0.5 (50% increase) in PE_2, η triples from *ca.* 14 to 42, which also triples σ from *ca.* 100 to 300 S cm^{-1}.

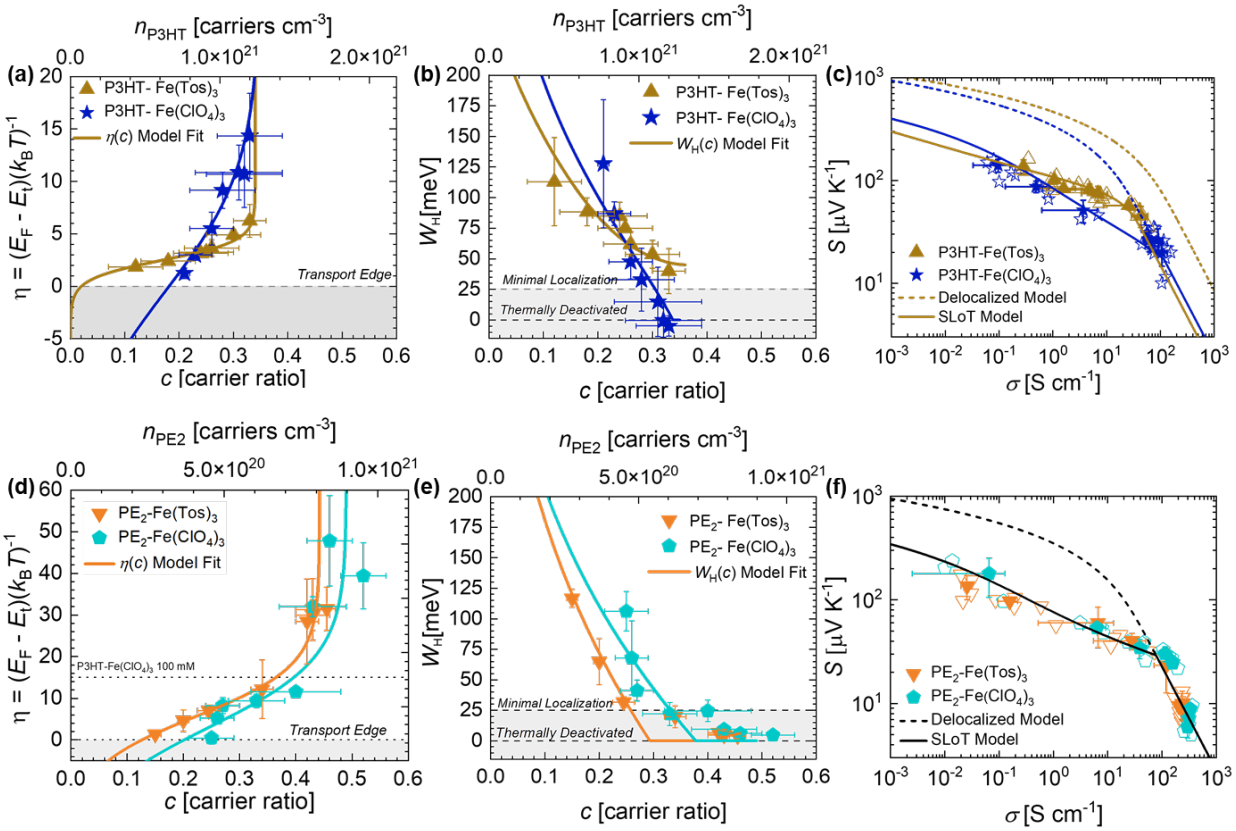

Figure 6: SLoT model analysis of P3HT and PE_2 doped with $Fe(Tos)_3$ and $Fe(ClO_4)_3$ solution concentrations. Individual data points represent doping level average measurements, error bars represent ± one standard deviation from multiple films, and solid lines represent SLoT model regressions. (a) P3HT and (d) PE_2 reduced Fermi energy level as a function of the carrier concentration. The transport edge is labeled at $\eta = 0$ and represents the onset of electronic transport within the context of the SLoT model. Note that panels (a) and (d) have the same x-axis but different y-axis scales. In panel (d), the P3HT-$Fe(ClO_4)_3$ 100 mM level is also denoated to help draw comparisons with panel (a). (b) P3HT and (e) PE_2 activation energies as a function of the carrier concentration ratio. Activation energy is considered to be minimal when $W_H < k_BT$, and transport is considered to be thermally deactivated when $W_H < 0$; both of these tresholds are labeled and represented by a dashed line. (c) P3HT and (f) PE_2 S-σ plots. Individual data points are represented by open data points, and doping level averages are represnted by filled data points. Dashed lines represent a delocalized curve (Kang-Snyder $s = 1$ curve), and solid lines represent SLoT model curves, calculated with no freely adjustable paramters. Measured data points and the modeled SLoT curve approach colinearity with the delocalized curve when $W_H < k_BT$. Source data, additional notes for calculating SLoT parameters, and error propogations are in **SLoT Model-P3HT and PE2 Study.xlsx** and **Notes S7,8.**

Table 1: SLoT Transport Parameters for P3HT and PE_2. c_t is the carrier ratio needed for the reduced Fermi energy level to be greater than the transport edge. $W_{H,slope}$ and $W_{H,max}$ determine the localization energy at any carrier ratio. c_d is the carrier ratio such that $W_H(c_d) = 0$. c_{max} is the maximum carrier ratio, calculated from XPS measurements. η_{max} is the maximum average reduced Fermi energy level calculated. μ_{max} is the maximum average carrier mobility. σ_{max} is the measured maximum electrical conductivity at a doping level, averaged from at least three unique films. Finally, σ_0 is the doping independent prefactor for the SLoT model. Additional notes for calculating SLoT parameters, nonlinear regression, and error propogations are in **SLoT Model-P3HT and PE2 Study.xlsx** and **Notes S7,8**.

	c_t	$W_{H,max}$ [meV]	$W_{H,slope}$ [meV]	c_d	c_{max}	η_{max}	μ_{max} [$cm^2V^{-1}s^{-1}$]	σ_{max} [S cm^{-1}]	σ_0 [S cm^{-1}]
P3HT-Fe(Tos)$_3$	0.020	290	350	n/a	0.33 ± 0.03	6.3	0.23	44	30
P3HT-Fe(ClO_4)$_3$	0.18	670	970	0.33	0.33 ± 0.06	14	0.56	107	7
PE_2-Fe(Tos)$_3$	0.13	600	900	0.29	0.46 ± 0.02	32	1.8	250	8
PE_2-Fe(ClO_4)$_3$	0.20	580	800	0.38	0.52 ± 0.04	48	2.5	330	10

3. Conclusion

This study compared the doping susceptibility and transport properties of P3HT and PE_2, with a variety of iron(III) salts at different concentrations. Among the salts studied, $Fe(ClO_4)_3$ imparted P3HT with the highest electrical conductivities, lowest Seebeck coefficients, and largest polaronic absorptions while $Fe(Tos)_3$ yielded the lowest electrical conductivities, highest Seebeck coefficients, and weakest polaronic absorptions, despite having comparable charge carrier densities. This indicates that the choice of charge balancing dopant anion can significantly affect charge transport properties. For PE_2, which is more disordered, easier to oxidize, and can support a higher carrier ratio compared to P3HT, the differences between $Fe(Tos)_3$ and $Fe(ClO_4)_3$ are less evident.

Using the SLoT model, we quantified how the charge carriers contributed to the observable transport properties. P3HT-$Fe(ClO_4)_3$ obtains higher reduced Fermi energy levels in comparison to P3HT-$Fe(Tos)_3$, likely due to thiophene oxide formation and its reduced aromaticity and increased propensity for quinoidal character. Additionally, at high doping levels, P3HT-$Fe(ClO_4)_3$ exhibits characteristics of delocalized transport while P3HT-$Fe(Tos)_3$ does not, likely because the tosylate ion disrupts the microstructure to a greater extent. Ultimately, P3HT-$Fe(ClO_4)_3$ achieves larger electrical conductivities and lower Seebeck coefficients in the highly doped limit (*ca.* 107 S cm^{-1} and +20 μV K^{-1} at 100 mM). In contrast, PE_2 doped with either $Fe(Tos)_3$ or $Fe(ClO_4)_3$ achieves similar transport properties and can be modeled sufficiently well using the same curve on the S-σ plot. At the high doping limit, PE_2-$Fe(ClO_4)_3$ achieves transport properties of 314 S cm^{-1} and +7.2 μV K^{-1} at 12 mM, which is 10 times more dilute than that used in P3HT. A thorough transport analysis suggests that PE_2-$Fe(ClO_4)_3$ achieves higher electrical conductivities and lower Seebeck coefficients than P3HT-$Fe(ClO_4)_3$ because the PE_2-$Fe(ClO_4)_3$ system can achieve higher extents of electrical oxidation (more charge carriers) and higher reduced Fermi energy levels.

For future studies, it should be noted that the dopant counterion chemistry can significantly alter the resulting transport properties. Additionally, increasing the extent of oxidation and/or the extent of

ordering (particularly in the neutral state) are likely good approaches towards high electrical conductivities, this study shows that these parameters do not necessarily guarantee an increase. Although PE_2 is solution processible, achieves 3-6 times higher electrical conductivities and is more susceptible to doping compared to P3HT, PE_2 obtains low Seebeck coefficients, and low thermoelectric power factors comparable to P3HT ($\sim 10\ \mu W\ m^{-1}\ K^{-2}$); therefore PE_2 is likely not advantageous for thermoelectric devices, akin to P3HT. However, PE_2 is a promising candidate for bioelectronic and transport conductor applications because of its enhanced electrical conductivity and susceptibility to doping. Finally, we note that the SLoT model provides a quantitative language for fundamental charge transport parameters ($e.g.$, $c_t, c_d, W_{\mathrm{H}}(c), \eta(c), \sigma_0$), that is the bedrock for developing future predictive design guidelines, and multiscale modeling, and structure-property relationships.

ASSOCIATED CONTENT

Instrumentation details, along with additional figures and tables, can be found in the Supporting Information. The Supporting Information is available free of charge at…

AUTHOR INFORMATION

Corresponding Author

*E-mails: Seth.Marder@nrel.gov and shannon.yee@me.gatech.edu

Author Contributions

K.A. led XPS, FTIR, UV-Vis-NIR, NMR, and CV measurements. S.A.G. led thermoelectric measurements and charge transport analysis. K.A. and S.A.G. led manuscript authorship with feedback and approval from all coauthors. M.P.G. coordinated GIWAXS measurements and analyzed GIWAXS data. J.F.P. provided experimental guidance throughout the project, prepared PE_2 films, and performed additional polymer characterizations. A.A. and J.M.R. assisted with thermoelectric measurements, profilometry, and contributed to the writing of this manuscript. A.L.J. synthesized the PE2 used for this study and provided additional PE2 characterization. J.J.U. advised M.P.G. with GIWAXS analysis. J.R.R. provided substantial manuscript feedback. S.B. and S.R.M. assisted in analyzing data, advising K.A., assisted in data analysis and editing the manuscript. S.K.Y. initially motivated this project and provided substantial feedback while preparing this manuscript.

ORCID

Khaled Al Kurdi: 0000-0001-9278-8162

Shawn A. Gregory: 0000-0002-1027-0675

Madeleine P. Gordon: 0000-0002-2818-7458

James F. Ponder Jr.: 0000-0001-8093-1849

Amalie Atassi: 0000-0003-3218-680X

Joshua M. Rinehart: 0000-0001-8111-27-49

Austin L. Jones: 0000-0002-3035-6548

Jeffrey J. Urban: 0000-0002-6520-830X

John R. Reynolds: 0000-0002-7417-4869

Stephen Barlow: 0000-0001-9059-9974

Seth R. Marder: 0000-0001-6921-2536

Shannon K. Yee: 0000-0002-1119-9938

Conflict of Interests:

There are no conflicts to declare.

Acknowledgements

K.A., S.B., and S.R.M. acknowledge support from the National Science Foundation (through the DMREF program DMR-1729737. S.A.G. appreciates the partial support from the Office of Naval Research (award no. N00014-19-1-2162), the Link Energy Foundation, and the Science and Technology of Material Interfaces (STAMI) group at the Georgia Institute of Technology. M.P.G gratefully acknowledges support from the National Science Foundation (NSF) Graduate Research Fellowship. J.M.R. is grateful for partial support from the Office of Naval Research (award no. N00014-19-1-2162) and the GAANN program at Georgia Institute of Technology (award no. P200A180075). A.A. appreciates the support from the National Science Foundation (NSF) Graduate Research Fellowship. S.K.Y. and J.R.R are grateful for partial support from the Office of Naval Research (awards no. N00014-19-1-2162 and N00014-20-1-2129, respectively). Any opinions, findings and conclusions or recommendations expressed in this material are those of the authors and do not necessarily reflect the views of the NSF.

Part of this work (XPS analysis) was performed in part at the Georgia Tech Institute for Electronics and Nanotechnology, a member of the National Nanotechnology Coordinated Infrastructure, which is supported by the NSF (grant no. ECCS-1542174). Part of this work (GIWAXS) was performed at the Molecular Foundry and the Advanced Light Source (beamline 7.3.3), Lawrence Berkeley National Laboratory, and was supported by the Department of Energy, Office of Science,

Office of Basic Energy Sciences, Scientific User Facilities Division of the U.S. Department of Energy under Contract No. DE-AC02-05CH11231.

References:

1. Ratcliff, E. L.; Jenkins, J. L.; Nebesny, K.; Armstrong, N. R., Electrodeposited, "Textured" Poly(3-Hexyl-Thiophene) (E-P3ht) Films for Photovoltaic Applications. *Chem. Mater.* **2008,** *20* (18), 5796-5806.
2. Al Kurdi, K.; McCarthy, D. P.; McMeekin, D. P.; Furer, S. O.; Tremblay, M.-H.; Barlow, S.; Bach, U.; Marder, S. R., A Naphthalene Diimide Side-Chain Polymer as an Electron-Extraction Layer for Stable Perovskite Solar Cells. *Mater. Chem. Front.* **2020,** *5*, 450-457.
3. Tremblay, M.-H.; Schutt, K.; Zhang, Y.; Lim, J.; Lin, Y.-H.; Warby, J. H.; Barlow, S.; Snaith, H. J.; Marder, S. R., A Photo-Crosslinkable Bis-Triarylamine Side-Chain Polymer as a Hole-Transport Material for Stable Perovskite Solar Cells. *Sustainable Energy Fuels* **2020,** *4* (1), 190-198.
4. Sirringhaus, H., 25th Anniversary Article: Organic Field-Effect Transistors: The Path Beyond Amorphous Silicon. *Adv. Mater.* **2014,** *26* (9), 1319-1335.
5. Bubnova, O.; Berggren, M.; Crispin, X., Tuning the Thermoelectric Properties of Conducting Polymers in an Electrochemical Transistor. *J. Am. Chem. Soc.* **2012,** *134* (40), 16456-16459.
6. Wang, S.; Ha, M.; Manno, M.; Daniel Frisbie, C.; Leighton, C., Hopping Transport and the Hall Effect near the Insulator-Metal Transition in Electrochemically Gated Poly(3-Hexylthiophene) Transistors. *Nat. Commun.* **2012,** *3*, 1210.
7. Russ, B.; Glaudell, A.; Urban, J. J.; Chabinyc, M. L.; Segalman, R. A., Organic Thermoelectric Materials for Energy Harvesting and Temperature Control. *Nat. Rev. Mater.* **2016,** *1* (10), 16050.
8. Pittelli, S. L.; De Keersmaecker, M.; Ponder Jr, J. F.; Österholm, A. M.; Ochieng, M. A.; Reynolds, J. R., Structural Effects on the Charge Transport Properties of Chemically and Electrochemically Doped Dioxythiophene Polymers. *J. Mater. Chem. C* **2020,** *8* (2), 683-693.
9. Ponder Jr., J. F.; Menon, A. K.; Dasari, R. R.; Pittelli, S. L.; Thorley, K. J.; Yee, S. K.; Marder, S. R.; Reynolds, J. R., Conductive, Solution-Processed Dioxythiophene Copolymers for Thermoelectric and Transparent Electrode Applications. *Adv. Energy Mater.* **2019,** *9* (24), 1900395.
10. Österholm, A. M.; Ponder, J. F.; De Keersmaecker, M.; Shen, D. E.; Reynolds, J. R., Disentangling Redox Properties and Capacitance in Solution-Processed Conjugated Polymers. *Chem. Mater.* **2019,** *31* (8), 2971-2982.
11. Vijayakumar, V.; Zhong, Y.; Untilova, V.; Bahri, M.; Herrmann, L.; Biniek, L.; Leclerc, N.; Brinkmann, M., Bringing Conducting Polymers to High Order: Toward Conductivities Beyond 105 S Cm−1 and Thermoelectric Power Factors of 2 Mw M−1 K−2. *Adv. Energy Mater.* **2019,** *9* (24), 1900266.
12. Bubnova, O.; Khan, Z. U.; Malti, A.; Braun, S.; Fahlman, M.; Berggren, M.; Crispin, X., Optimization of the Thermoelectric Figure Of merit in the Conducting Polymer Poly(3,4-Ethylenedioxythiophene). *Nat. Mater.* **2011,** *10* (6), 429-433.
13. Xuan, Y.; Liu, X.; Desbief, S.; Leclère, P.; Fahlman, M.; Lazzaroni, R.; Berggren, M.; Cornil, J.; Emin, D.; Crispin, X., Thermoelectric Properties of Conducting Polymers: The Case of Poly(3-Hexylthiophene). *Phys. Rev. B* **2010,** *82* (11), 115454.
14. Wegner, B.; Lungwitz, D.; Mansour, A. E.; Tait, C. E.; Tanaka, N.; Zhai, T.; Duhm, S.; Forster, M.; Behrends, J.; Shoji, Y.; Opitz, A.; Scherf, U.; List-Kratochvil, E. J. W.; Fukushima, T.; Koch, N., An Organic Borate Salt with Superior P-Doping Capability for Organic Semiconductors. *Advanced Science* **2020,** *7* (17), 2001322.

15. Gregory, S. A.; Menon, A. K.; Ye, S.; Seferos, D. S.; Reynolds, J. R.; Yee, S. K., Effect of Heteroatom and Doping on the Thermoelectric Properties of Poly(3-Alkylchalcogenophenes). *Adv. Energy Mater.* **2018,** *8* (34), 1-8.
16. Kang, K.; Schott, S.; Venkateshvaran, D.; Broch, K.; Schweicher, G.; Harkin, D.; Jellett, C.; Nielsen, C. B.; McCulloch, I.; Sirringhaus, H., Investigation of the Thermoelectric Response in Conducting Polymers Doped by Solid-State Diffusion. *Materials Today Physics* **2019,** *8*, 112-122.
17. Hisaaki Tanaka, K. K., Naoya Takekoshi, Hiroaki Mada, Hiroshi Ito, Yukihiro Shimoi, Hiromichi Ohta, Taishi Takenobu, Thermoelectric Properties of a Semicrystalline Polymer Doped Beyond the Insulator-to-Metal Transition by Electrolyte Gating. *Sci. Adv.* **2020,** *6*, 1-8.
18. Reynolds, J. R.; Thompson, B. C.; Skotheim, T. A., *Handbook of Conducting Polymers*. 1998.
19. Bargigia, I.; Savagian, L. R.; Österholm, A. M.; Reynolds, J. R.; Silva, C., Charge-Transfer Intermediates in the Electrochemical Doping Mechanism of Conjugated Polymers. *J. Am. Chem. Soc.* **2021,** *143* (1), 294-308.
20. Pittelli, S. L.; Gregory, S. A.; Ponder, J. F.; Yee, S. K.; Reynolds, J. R., Inducing Planarity in Redox-Active Conjugated Polymers with Solubilizing 3,6-Dialkoxy-Thieno[3,2-B]Thiophenes (Dotts) for Redox and Solid-State Conductivity Applications. *J. Mater. Chem. C* **2020,** *8* (22), 7463-7475.
21. Jones, A. L.; De Keersmaecker, M.; Pelse, I.; Reynolds, J. R., Curious Case of Biedot: Maldi-Tof Mass Spectrometry Reveals Unbalanced Monomer Incorporation with Direct (Hetero)Arylation Polymerization. *Macromolecules* **2020,** *53* (17), 7253-7262.
22. Ponder, J. F.; Österholm, A. M.; Reynolds, J. R., Designing a Soluble Pedot Analogue without Surfactants or Dispersants. *Macromolecules* **2016,** *49* (6), 2106-2111.
23. Gregory, S. A.; Ponder, J. F.; Pittelli, S. L.; Losego, M. D.; Reynolds, J. R.; Yee, S. K., Thermoelectric and Charge Transport Properties of Solution-Processable and Chemically Doped Dioxythienothiophene Copolymers. *ACS Applied Polymer Materials* **2021,** *3*, 2316-2324.
24. Mazaheripour, A.; Thomas, E. M.; Segalman, R. A.; Chabinyc, M. L., Nonaggregating Doped Polymers Based on Poly(3,4-Propylenedioxythiophene). *Macromolecules* **2019,** *52* (5), 2203-2213.
25. Ponder, J. F., Jr.; Gregory, S. A.; Atassi, A.; Menon, A. K.; Lang, A. W.; Savagian, L. R.; Reynolds, J. R.; Yee, S. K., Significant Enhancement of the Electrical Conductivity of Conjugated Polymers by Post-Processing Side Chain Removal. *J Am Chem Soc* **2022,** *144*, 1351-1360.
26. Thomas, E. M.; Peterson, K. A.; Balzer, A. H.; Rawlings, D.; Stingelin, N.; Segalman, R. A.; Chabinyc, M. L., Effects of Counter-Ion Size on Delocalization of Carriers and Stability of Doped Semiconducting Polymers. *Adv. Electron. Mater.* **2020,** *6* (12), 2000595.
27. Un, H.-I.; Gregory, S. A.; Mohapatra, S. K.; Xiong, M.; Longhi, E.; Lu, Y.; Rigin, S.; Jhulki, S.; Yang, C.-Y.; Timofeeva, T. V.; Wang, J.-Y.; Yee, S. K.; Barlow, S.; Marder, S. R.; Pei, J., Understanding the Effects of Molecular Dopant on N-Type Organic Thermoelectric Properties. *Adv. Energy Mater.* **2019,** *9* (24), 1900817.
28. Fontana, M. T.; Stanfield, D. A.; Scholes, D. T.; Winchell, K. J.; Tolbert, S. H.; Schwartz, B. J., Evaporation Vs Solution Sequential Doping of Conjugated Polymers: F4tcnq Doping of Micrometer-Thick P3ht Films for Thermoelectrics. *The Journal of Physical Chemistry C* **2019,** *123* (37), 22711-22724.
29. Jacobs, I. E.; Lin, Y.; Huang, Y.; Ren, X.; Simatos, D.; Chen, C.; Tjhe, D.; Statz, M.; Lai, L.; Finn, P. A.; Neal, W. G.; D'Avino, G.; Lemaur, V.; Fratini, S.; Beljonne, D.; Strzalka, J.; Nielsen, C. B.; Barlow, S.; Marder, S. R.; McCulloch, I.; Sirringhaus, H., High-Efficiency Ion-Exchange Doping of Conducting Polymers. *Adv Mater* **2021**, e2102988.
30. Stanfield, D. A.; Wu, Y.; Tolbert, S. H.; Schwartz, B. J., Controlling the Formation of Charge Transfer Complexes in Chemically Doped Semiconducting Polymers. *Chem. Mater.* **2021,** *33* (7), 2343-2356.
31. Hagen, K. S., Iron(Ii) Triflate Salts as Convenient Substitutes for Perchlorate Salts: Crystal Structures of [Fe(H2o)6](Cf3so3)2 and Fe(Mecn)4(Cf3so3)2. *Inorg. Chem.* **2000,** *39* (25), 5867-5869.

32. Wulfsberg, G.; Parks, K. D.; Rutherford, R.; Jackson, D. J.; Jones, F. E.; Derrick, D.; Ilsley, W.; Strauss, S. H.; Miller, S. M.; Anderson, O. P.; Babushkina, T. A.; Gushchin, S. I.; Kravchenko, E. A.; Morgunov, V. G., Weakly Coordinating Anions: Crystallographic and Nqr Studies of Halogen−Metal Bonding in Silver, Thallium, Sodium, and Potassium Halomethanesulfonates. *Inorg. Chem.* **2002,** *41* (8), 2032-2040.
33. Strauss, S. H., The Search for Larger and More Weakly Coordinating Anions. *Chem. Rev.* **1993,** *93* (3), 927-942.
34. Yamashita, Y.; Tsurumi, J.; Ohno, M.; Fujimoto, R.; Kumagai, S.; Kurosawa, T.; Okamoto, T.; Takeya, J.; Watanabe, S., Efficient Molecular Doping of Polymeric Semiconductors Driven by Anion Exchange. *Nature* **2019,** *572* (7771), 634-638.
35. Watanabe, S.; Ohno, M.; Yamashita, Y.; Terashige, T.; Okamoto, H.; Takeya, J., Validity of the Mott Formula and the Origin of Thermopower in Π-Conjugated Semicrystalline Polymers. *Phys. Rev. B* **2019,** *100* (24), 1-8.
36. Long, N., *Metallocenes: An Introduction to Sandwich Complexes*. 1 ed.; Wiley-Blackwell: 1998; p 285.
37. Reynolds, J., R. ; Chien, J. C. W.; Karasz, F. E.; Lillya, C. P.; Curran, D. J., Iron(Iii) Perchlorate Doping of Polyacetylene. *J. Chem. Soc., Chem. Commun.* **1982,** (23), 1358-1359.
38. Wu, L.; Li, H.; Chai, H.; Xu, Q.; Chen, Y.; Chen, L., Anion-Dependent Molecular Doping and Charge Transport in Ferric Salt-Doped P3ht for Thermoelectric Application. *ACS Appl. Electron. Mater.* **2021,** *3* (3), 1252-1259.
39. Mott, N. F.; Davis, E. A., *Electronic Processes in Non-Crystalline Materials*. Oxford University Press: 2012.
40. Gregory, S. A.; Hanus, R.; Atassi, A.; Rinehart, J. M.; Wooding, J. P.; Menon, A. K.; Losego, M. D.; Snyder, G. J.; Yee, S. K., Quantifying Charge Carrier Localization in Chemically Doped Semiconducting Polymers. *Nat. Mater.* **2021,** *20*, 1414-1421.
41. Wynne, K. J.; Street, G. B., Poly(Pyrrol-2-Ylium Tosylate): Electrochemical Synthesis and Physical and Mechanical Properties. *Macromolecules* **1985,** *18*, 23611-2368.
42. Pittelli, S. L.; Shen, D. E.; Osterholm, A. M.; Reynolds, J. R., Chemical Oxidation of Polymer Electrodes for Redox Active Devices: Stabilization through Interfacial Interactions. *ACS. Appl. Mater. Interfaces* **2018,** *10* (1), 970-978.
43. Shallcross, R. C.; Stubhan, T.; Ratcliff, E. L.; Kahn, A.; Brabec, C. J.; Armstrong, N. R., Quantifying the Extent of Contact Doping at the Interface between High Work Function Electrical Contacts and Poly(3-Hexylthiophene) (P3ht). *J. Phys. Chem. Lett.* **2015,** *6* (8), 1303-1309.
44. Jenkins, J. L.; Lee, P. A.; Nebesny, K. W.; Ratcliff, E. L., Systematic Electrochemical Oxidative Doping of P3ht to Probe Interfacial Charge Transfer across Polymer–Fullerene Interfaces. *J. Mater. Chem. A* **2014,** *2* (45), 19221-19231.
45. Buckingham, M. A.; Marken, F.; Aldous, L., The Thermoelectrochemistry of the Aqueous Iron(Ii)/Iron(Iii) Redox Couple: Significance of the Anion and Ph in Thermogalvanic Thermal-to-Electrical Energy Conversion. *Sustainable Energy Fuels* **2018,** *2* (12), 2717-2726.
46. Moseki, Y.; Sayama, K., High-Efficiency Water Oxidation and Energy Storage Utilizing Various Reversible Redox Mediators under Visible Light over Surface-Modified Wo3. *RSC Adv.* **2014,** *4*, 8308-8316.
47. Shakirullah, M.; Ahmad, W.; Ahmad, I.; Ishaq, M., Oxidative Desulphurization Study of Gasoline and Kerosene: Role of Some Organic and Inorganic Oxidants. *Fuel Process. Technol.* **2010,** *91* (11), 1736-1741.
48. Zevalkink, A.; Smiadak, D. M.; Blackburn, J. L.; Ferguson, A. J.; Chabinyc, M. L.; Delaire, O.; Wang, J.; Kovnir, K.; Martin, J.; Schelhas, L. T.; Sparks, T. D.; Kang, S. D.; Dylla, M. T.; Snyder, G. J.; Ortiz, B. R.; Toberer, E. S., A Practical Field Guide to Thermoelectrics: Fundamentals, Synthesis, and Characterization. *Appl. Phys. Rev.* **2018,** *5* (2), 021303.

49. Kang, S. D.; Snyder, G. J., Charge-Transport Model for Conducting Polymers. *Nat. Mater.* **2017,** *16* (2), 252-257.
50. Snyder, G. J.; Snyder, A. H.; Wood, M.; Gurunathan, R.; Snyder, B. H.; Niu, C., Weighted Mobility. *Adv. Mate.r* **2020,** *32* (25), e2001537.
51. Kelley, A. M., *Condensed-Phase Molecular Spectroscopy and Photophysics* 2012; p 344.
52. Milanovich, M.; Sarkar, T.; Popowski, Y.; Low, J. Z.; Campos, L. M.; Kenig, S.; Frey, G. L.; Amir, E., Enhancing P3ht/Pcbm Blend Stability by Thermal Crosslinking Using Poly(3-Hexylthiophene)-S,S-Dioxide. *J. Mater. Chem. C* **2020,** *8* (23), 7698-7707.
53. Marrikar, F. S.; Brumbach, M.; Evans, D. H.; Lebrón-Paler, A.; Pemberton, J. E.; Wysocki, R. J.; Armstrong, N. R., Modification of Indium−Tin Oxide Electrodes with Thiophene Copolymer Thin Films: Optimizing Electron Transfer to Solution Probe Molecules. *Langmuir* **2007,** *23* (3), 1530-1542.
54. Mitraka, E.; Jafari, M. J.; Vagin, M.; Liu, X.; Fahlman, M.; Ederth, T.; Berggren, M.; Jonsson, M. P.; Crispin, X., Oxygen-Induced Doping on Reduced Pedot. *J. Mater. Chem. A* **2017,** *5* (9), 4404-4412.
55. Marciniak, S.; Crispin, X.; Uvdal, K.; Trzcinski, M.; Birgerson, J.; Groenendaal, L.; Louwet, F.; Salaneck, W. R., Light Induced Damage in Poly(3,4-Ethylenedioxythiophene) and Its Derivatives Studied by Photoelectron Spectroscopy. *Synth. Met.* **2004,** *141* (1), 67-73.
56. Crispin, X.; Marciniak, S.; Osikowicz, W.; Zotti, G.; van der Gon, A. W. D.; Louwet, F.; Fahlman, M.; Groenendaal, L.; De Schryver, F.; Salaneck, W. R., Conductivity, Morphology, Interfacial Chemistry, and Stability of Poly(3,4-Ethylene Dioxythiophene)–Poly(Styrene Sulfonate): A Photoelectron Spectroscopy Study. *J. Polym. Sci., Part B: Polym. Phys.* **2003,** *41* (21), 2561-2583.
57. Khan, Z. U.; Bubnova, O.; Jafari, M. J.; Brooke, R.; Liu, X.; Gabrielsson, R.; Ederth, T.; Evans, D. R.; Andreasen, J. W.; Fahlman, M.; Crispin, X., Acido-Basic Control of the Thermoelectric Properties of Poly(3,4-Ethylenedioxythiophene)Tosylate (Pedot-Tos) Thin Films. *J. Mater. Chem. C* **2015,** *3* (40), 10616-10623.
58. Shi, W.; Yao, Q.; Qu, S.; Chen, H.; Zhang, T.; Chen, L., Micron-Thick Highly Conductive Pedot Films Synthesized Via Self-Inhibited Polymerization: Roles of Anions. *NPG Asia Mater.* **2017,** *9* (7), e405-e405.
59. Neusser, D.; Malacrida, C.; Kern, M.; Gross, Y. M.; van Slageren, J.; Ludwigs, S., High Conductivities of Disordered P3ht Films by an Electrochemical Doping Strategy. *Chem. Mater.* **2020,** *32* (14), 6003-6013.
60. Dong, B. X.; Nowak, C.; Onorato, J. W.; Ma, T.; Niklas, J.; Poluektov, O. G.; Grocke, G.; DiTusa, M. F.; Escobedo, F. A.; Luscombe, C. K.; Nealey, P. F.; Patel, S. N., Complex Relationship between Side-Chain Polarity, Conductivity, and Thermal Stability in Molecularly Doped Conjugated Polymers. *Chem. Mater.* **2021,** *33* (2), 741-753.
61. Durand, P.; Zeng, H.; Biskup, T.; Vijayakumar, V.; Untilova, V.; Kiefer, C.; Heinrich, B.; Herrmann, L.; Brinkmann, M.; Leclerc, N., Single Ether-Based Side Chains in Conjugated Polymers: Toward Power Factors of 2.9 mw M −1 K −2. *Adv. Energy Mater.* **2021,** *12* (2103049), 1-11.
62. Conboy, G.; Spencer, H. J.; Angioni, E.; Kanibolotsky, A. L.; Findlay, N. J.; Coles, S. J.; Wilson, C.; Pitak, M. B.; Risko, C.; Coropceanu, V.; Brédas, J.-L.; Skabara, P. J., To Bend or Not to Bend – Are Heteroatom Interactions within Conjugated Molecules Effective in Dictating Conformation and Planarity? *Mater. Horiz.* **2016,** *3* (4), 333-339.
63. Gordon, M. P.; Gregory, S. A.; Wooding, J. P.; Ye, S.; Su, G. M.; Seferos, D. S.; Losego, M. D.; Urban, J. J.; Yee, S. K.; Menon, A. K., Microstructure and Heteroatom Dictate the Doping Mechanism and Thermoelectric Properties of Poly(Alkyl-Chalcogenophenes). *Appl. Phys. Lett.* **2021,** *118* (23), 1-8.
64. Kim, E. G.; Coropceanu, V.; Gruhn, N. E.; Sanchez-Carrera, R. S.; Snoeberger, R.; Matzger, A. J.; Bredas, J. L., Charge Transport Parameters of the Pentathienoacene Crystal. *J. Am. Chem. Soc.* **2007,** *129* (43), 13072-81.

65. Meysam Heydari Gharahcheshmeh, M. M. T., Edward F. Gleason, Maxwell T. Robinson, Jing Kong, Karen K. Gleason, Tuning, Optimization, and Perovskite Solar Cell Device Integration of Ultrathin Poly(3,4-Ethylene Dioxythiophene) Films Via a Single-Step All-Dry Process. *Sci. Adv.* **2019,** *5*, 1-12.
66. Bubnova, O.; Khan, Z. U.; Wang, H.; Braun, S.; Evans, D. R.; Fabretto, M.; Hojati-Talemi, P.; Dagnelund, D.; Arlin, J. B.; Geerts, Y. H.; Desbief, S.; Breiby, D. W.; Andreasen, J. W.; Lazzaroni, R.; Chen, W. M.; Zozoulenko, I.; Fahlman, M.; Murphy, P. J.; Berggren, M.; Crispin, X., Semi-Metallic Polymers. *Nat. Mater.* **2014,** *13* (2), 190-4.
67. Thomas, E. M.; Davidson, E. C.; Katsumata, R.; Segalman, R. A.; Chabinyc, M. L., Branched Side Chains Govern Counterion Position and Doping Mechanism in Conjugated Polythiophenes. *ACS Macro Lett.* **2018,** *7* (12), 1492-1497.
68. Pascale Pouzet; Irene Erdelmeier; Daria Ginderow; Jean-Paul Mornon; Patrick Dansettea; Mansuy, D., Thiophene S-Oxides: Convenient Preparation, First Complete Structural Characterization and Unexpected Dimerization of One of Them, 2,5-Diphenylthiophene-I -Oxide. *J. Chem. Soc. Chem. Comm.* **1995,** *4*, 473-474.
69. Zeier, W. G.; Zevalkink, A.; Gibbs, Z. M.; Hautier, G.; Kanatzidis, M. G.; Snyder, G. J., Thinking Like a Chemist: Intuition in Thermoelectric Materials. *Angew. Chem., Int. Ed. Engl.* **2016,** *55* (24), 6826-41.
70. Zeng, H.; Mohammed, M.; Untilova, V.; Boyron, O.; Berton, N.; Limelette, P.; Schmaltz, B.; Brinkmann, M., Fabrication of Oriented N-Type Thermoelectric Polymers by Polarity Switching in a Dpp-Based Donor–Acceptor Copolymer Doped with Fecl3. *Adv. Electron Mater.* **2021**, 1-14.